JOURNAL OF CATALYSIS 154, 245–252 (1995)

CO Hydrogenation to Higher Oxygenates over Promoted Rhodium: Nature of the Metal–Promoter Interaction in RhMn/NaY

Horacio Treviño, Guan-Dao Lei, and Wolfgang M. H. Sachtler

V. N. Ipatieff Laboratory, Center for Catalysis and Surface Science, Departments of Chemistry and Chemical Engineering, Northwestern University, Evanston, Illinois 60208

Received December 16, 1994; revised March 14, 1995

Unpromoted and manganese-promoted zeolite Y supported rhodium catalysts were tested for CO hydrogenation at 1 MPa and 250°C. The conditions of catalyst preparation by ion exchange, programmed calcination, programmed reduction and neutralization of acid sites were varied systematically in order to compare the promoter effects of different species of manganese. It is found that only MnO particles, and not Mn^{2+} ions, promote the Rh-catalyzed formation of the abundant oxygenates ethanol and ethyl acetate. No reduction in Mn^0 or Rh–Mn alloy formation takes place. Temperature-programmed reduction profiles of Mn/NaY and RhMn/NaY show that reduction of MnO_2 to MnO is dramatically enhanced by Rh, indicating that in the reduced catalyst Rh clusters and MnO clusters are in physical contact. Direct interaction between Rh and MnO also follows from EXAFS data which show that the Rh–Rh coordination number is much lower in NaY when MnO particles are present. TPD results indicate that MnO affects the propensity of Rh to chemisorb hydrogen. Tentative reaction mechanisms for CO hydrogenation are considered, consistent with the experimental findings. © 1995 Academic Press, Inc.

INTRODUCTION

For the hydrogenation of carbon monoxide, rhodium is one of the most versatile catalysts (1–4). It has the capability to adsorb CO both dissociatively and nondissociatively (5–7). Hydrogenation of CO over rhodium catalysts yields a wide variety of products, hydrocarbons, methanol, and higher oxygenates (1, 8–11). The product distributions depend strongly on the reaction conditions and, more importantly, on the presence and type of additional components of the catalyst, generally referred to as "promoters." A catalyst promoter is defined as an element or compound that has a negligible catalytic activity by itself, but when added to a catalyst it improves its activity or selectivity.

Some promoted rhodium catalysts are highly active and/or selective towards the formation of higher oxygenates in CO hydrogenation (12, 13). In the widely accepted mechanism (14), higher oxygenate formation requires dissociative adsorption of CO followed by alkyl chain growth via stepwise addition of CH_2 units, and nondissociative adsorption of CO which can be inserted at the end of the chain. Accordingly, the carbon atom of the nondissociatively adsorbed CO is found at the end of the molecule in the primary oxygenates (aldehydes, alcohols) (15). A variety of promoters are known, including alkali (16–17), rare earth (9, 18), and transition elements (19–23). Also the support can act as a promoter. Several models have been proposed on how promoters affect the selectivity for oxygenate formation of Rh and other metals (4, 14, 20, 24–26). Most of them assume a localized chemical interaction among metal, promoter, and reactants. Experimental verification of these models is problematic for unsupported catalysts and for rhodium supported on amorphous oxides. In the present work the opportunity of zeolite supports is exploited to obtain a better identification of the chemical nature of the promoter and its interaction with rhodium particles.

Manganese has been used as a promoter of rhodium, increasing its catalytic activity and, in some cases, the selectivity toward C_2 oxygenates, such as ethanol and acetic acid (12, 15, 31, 32). The rhodium–manganese pair has, therefore, been chosen for the present study; zeolite Y has been used to accomodate Rh_n^0 clusters and Mn in a variety of identifiable structures. Catalysts in which Mn is exclusively present as Mn^{2+} can be compared with those where all Mn is present as MnO particles. If alloy formation occurs, it can be identified, as was done previously with other bimetallic pairs in zeolite Y (33–35). The specific objective of the present work is to determine the chemical state in which Mn promotes the formation of higher oxygenates and to obtain information on the nature of the interaction between Rh and Mn.

EXPERIMENTAL

The catalysts were prepared by ion exchange in zeolite NaY (Union Carbide Lot No. 968087061020-5-8, kindly provided by the manufacturer) by adding dropwise a solu-

0021-9517/95 $12.00

tion of the appropriate precursor to a 5-g/liter zeolite doubly deionized water slurry. The precursors were $[Rh(NH_3)_5Cl]Cl_2$ and $Mn(NO_3)_2 \cdot 6H_2O$. After hydrolysis the ions are assumed to enter the zeolite as $[Rh(NH_3)_5H_2O]^{3+}$ and $[Mn(H_2O)_6]^{2+}$ ions. Further treatment included calcination in pure O_2, ramping the temperature at 0.5°C/min, and reduction in pure H_2 with a temperature ramp of 8°C/min. Elemental analysis confirmed the absence of chlorine in the reduced catalysts. In some samples the protons formed during reduction were neutralized by immersing the catalyst in a NaOH solution at pH 11. After this neutralization the catalyst was calcined and reduced again. Exposure of Mn^{2+} ions to a basic environment hydrolyzes them and, after calcination and reduction, manganese oxide, MnO, is formed.

For reaction studies a stainless steel fixed bed flow reactor was used with automatic control of temperature, pressure, and feed flow rate. Reduction was carried out *in situ*. After the reactor was pressurized under H_2, the syngas mixture was admitted to start the reaction. Unless stated otherwise, a total pressure of 1 MPa, a reaction temperature of 250°C, a CO/H_2 ratio of 1, and space velocities of 5000–9000 h^{-1} were used.

Temperature-programmed reduction (TPR) experiments were carried out in an open flow system with automatic flow control and equipped with a TCD cell. Reduction was done using an 8°C/min temperature ramp and a mixture of 5% H_2 in Ar, from −60 to 540°C. Temperature programmed desorption (TPD) experiments were always carried out after a TPR run in the same open flow system. The sample was cooled down under flowing 5% H_2/Ar and this flow continued for 15 min after reaching room temperature. After this, the flow was switched to pure Ar and the sample was kept for 15 min at room temperature. Then it was immersed in an acetone/dry ice bath. Temperature ramping (8°C/min) and data collection began at −60°C and stopped at 540°C.

FTIR experiments were done in a Nicolet 60SX system. The samples were pressed into self-supporting wafers and pretreated *in situ*. Spectra were taken at room temperature.

Rh *K*-edge (23.2 keV) EXAFS data were collected at the CHESS facility station C2 of the Wilson Laboratory at Cornell University (Ithaca, NY). The data were collected in the transmission mode at 25°C. The catalyst was calcined *ex situ* at 400°C in O_2, pressed into pellets, transferred in air, and reduced *in situ* at 400°C in a 20 ml/min flow of 5% H_2/He. The cell used is constructed of stainless steel and equipped with kapton film windows. The EXAFS data analysis was based on experimentally determined phase shifts and backscattering amplitudes of a structure standard Rh foil. The coordination number (CN) of Rh in the foil was taken as 12 with a nearest neighbor bond distance R_{Rh-Rh} of 0.268 nm. The data were processed using a PC-based EXAFS analysis program obtained from Tolmar Instruments (Hamilton, Ontario, Canada).

RESULTS

1. Reaction Studies

Hereafter the superscript N will be used to denote catalyst samples that were immersed in a NaOH solution after ion exchange. More specifically, Rh^NMn/NaY stands for a sample exposed to NaOH after Rh exchange, but prior to Mn exchange, and Rh^NMn^N/NaY is a catalyst exposed to NaOH after both Rh and Mn ion exchanges.

The following summarizes the results of catalytic reaction runs (32):

—With unpromoted Rh/NaY catalysts, both neutralized and nonneutralized, only hydrocarbons are produced, with methane as the main product.

—Promoted RhMn/NaY catalysts are selective towards higher oxygenate formation *only* after immersion in NaOH solution, as shown in Fig. 1. The main oxygenate products are ethanol and ethyl acetate.

—To determine the role of acidic zeolite protons, which are formed during the reduction of Rh, layered bed experiments were performed. Two catalyst beds, separated by an inert material such as glass wool, were loaded in the reactor. No oxygenates are observed in the effluent for several hours when a bed of zeolite HY, which has a high acid proton concentration, is loaded downstream from a bed of neutralized RhMn/NaY, which is selective towards higher oxygenates. If the sequence of catalyst beds is reversed the observed product distribution is approxi-

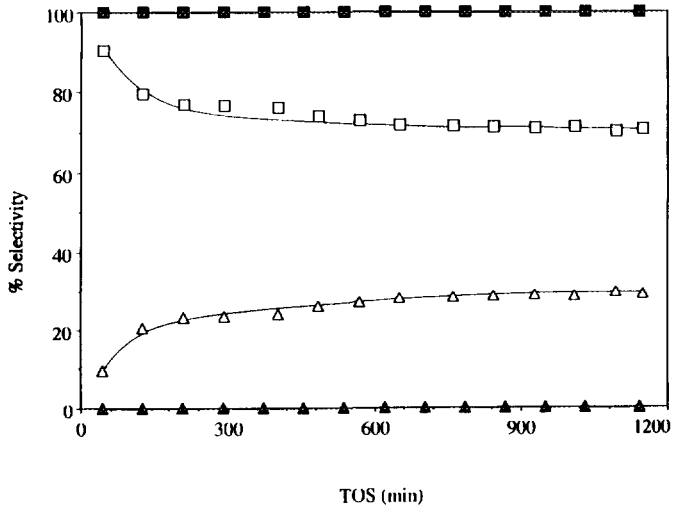

FIG. 1. Selectivity on a C atom basis towards different products plotted vs time on stream (TOS). RhMn/NaY nonneutralized: ■, hydrocarbons; ▲, oxygenates. RhMn/NaY NaOH-neutralized: □, hydrocarbons; △, oxygenates.

mately the same as when the neutralized RhMn/NaY is loaded alone in the reactor. This is shown in Fig. 2.

—Calcination at temperatures below 200°C does not destroy the ammine ligands of the Rh precursor. Whereas reduction of samples that have been calcined at 500°C produces three protons per Rh atom, no protons are produced in samples which were calcined at 200°C because the original ammine ligands immediately react with protons to give NH_4^+ ions.

Catalysts in which Mn ion exchange was followed by Rh ion exchange, calcination at 200°C, and reduction did not produce detectable amounts of oxygenates. In contrast, when the catalyst was immersed in NaOH after Mn ion exchange, but *prior* to Rh ion exchange, and then calcined at 200°C, a significant selectivity towards higher oxygenates was observed. This result is depicted in Fig. 3.

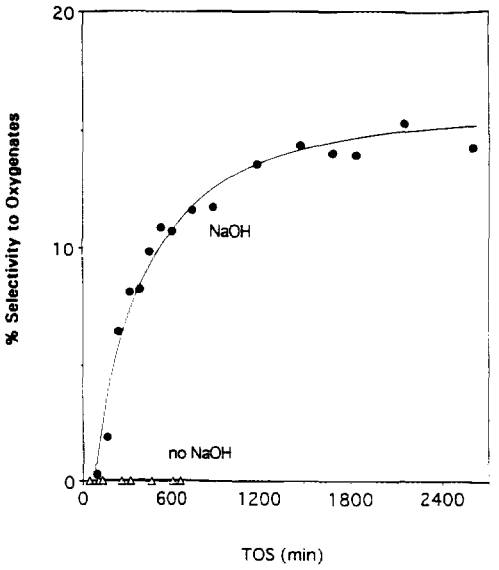

FIG. 3. Effect of NaOH immersion after Mn ion exchange but *prior* to Rh exchange. Selectivity of RhMn/NaY catalysts calcined at 200°C towards oxygenates plotted vs TOS. △, not exposed to NaOH; ●, exposed to NaOH.

2. *Temperature-Programmed Reduction*

The TPR profiles of Rh^N/NaY, Mn/NaY, Mn^N/NaY, Rh^NMn/NaY, and Rh^NMn^N/NaY are shown in Fig. 4, traces a through e, respectively. All experiments were run after calcining at 400°C under pure O_2.

The Rh^N/NaY sample has a single sharp peak at around 45°C, which is assigned to the reduction of Rh oxide RhO_2 or possibly a mixture of RhO_2 and Rh_2O_3 (36).

Mn/NaY does not show any reduction peak, implying that Mn^{2+} ions are not reducible under these conditions. This is in agreement with the thermodynamic parameters of this system.

The TPR profile of Mn^N/NaY is completely different. It has two main peaks at about 280 and 400°C, which can be ascribed to the stepwise reduction sequence $MnO_2 \rightarrow Mn_3O_4 \rightarrow MnO$.

The Rh^NMn/NaY sample has a TPR profile very similar to the Mn-free Rh^N/NaY sample. Only reduction of Rh oxide is observed. Again, there is no evidence of reduction of Mn^{2+} ions.

The TPR pattern of Rh^NMn^N/NaY significantly differs from the linear combinations of the TPR of Rh^N/NaY and Mn^N/NaY. There is a sharp peak at about 60°C, a shoulder at 115°C, and a smaller peak at 175°C. Clearly, Rh strongly affects the reduction of MnO_2.

3. *Temperature-Programmed Desorption*

The TPD spectra of the different samples show approximately the same peak positions. The main difference

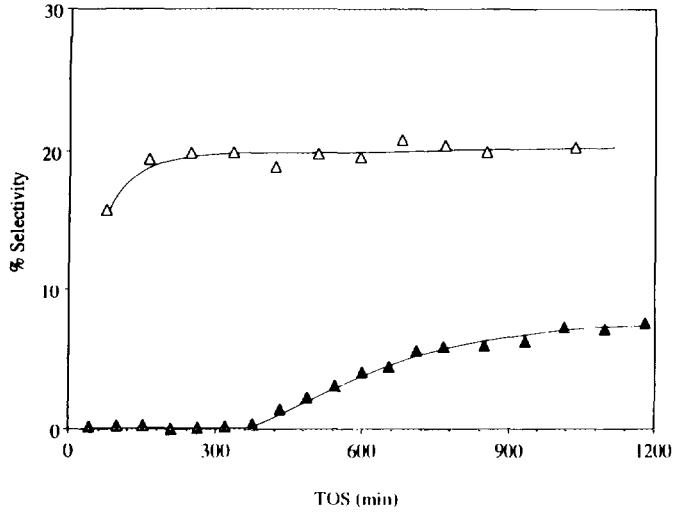

FIG. 2. Selectivity towards oxygenates in layered bed experiments plotted vs TOS. ▲, RhMn/NaY NaOH-neutralized → HY →. △, HY → RhMn/NaY NaOH-neutralized →.

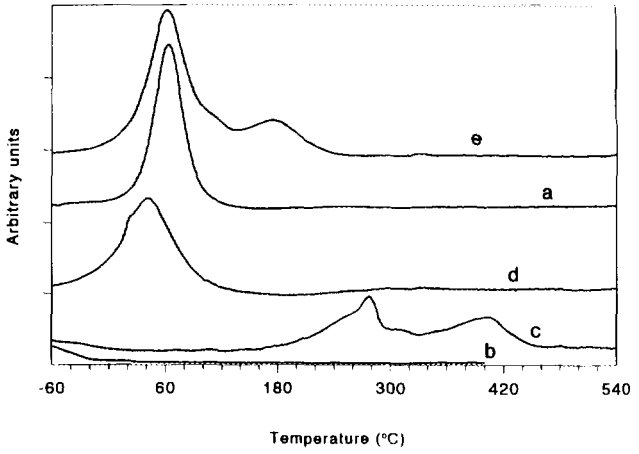

FIG. 4. TPR profiles at 8°C/min in 5% H_2/Ar of: (a) Rh^N/NaY, (b) Mn/NaY, (c) Mn^N/NaY, (d) Rh^NMn/NaY, and (e) Rh^NMn^N/NaY.

TABLE 1

H/Rh Ratios Measured by TPD of Different Catalysts

Catalyst	Rh^N/NaY	Rh^NMn/NaY	Rh^NMn^N/NaY
H/Rh	1.34	0.97	0.77

among the samples is the amount of hydrogen produced. The results are summarized in Table 1. The amount of hydrogen desorbed is lower when Mn is present and is lowest in the Rh^NMn^N/NaY catalyst.

4. FTIR Spectra

FTIR spectra of *in situ* reduced samples were taken upon admission of CO as a probe molecule to characterize the different species present in the zeolite cages.

(a) Rh^N/NaY after exposure to CO is shown in Fig. 5. The predominant species are $Rh_6(CO)_{16}$ clusters, which give rise to the bands at 1762, 1831, 1871, 2065, and 2091 cm^{-1} (37), and CO attached in both linear and bridged forms to larger Rh_n particles, which produces wide bumps in the 2050 and 1840 cm^{-1} regions. There is also a small amount of the *gem*-dicarbonyl $Rh^+(CO)_2$, as indicated by the pairs of bands at 2025 and 2099 cm^{-1}, and 2048 and 2117 cm^{-1}.

(b) Rh^NMn/NaY, where the protons formed after the reduction of Rh were neutralized with NaOH *before* the exchange of Mn, is shown in Fig. 6 after exposure to CO. The presence of $Rh_6(CO)_{16}$ is evident from the bands at 2099, 2072, 2090, 1866, and 1827 cm^{-1}. There is little evidence of the presence of the *gem*-dicarbonyl $Rh^+(CO)_2$. The band at 2053 cm^{-1} can be tentatively related to a band at 2052 cm^{-1} ascribed to an Rh^0 cluster. The most striking difference from the Mn-free sample

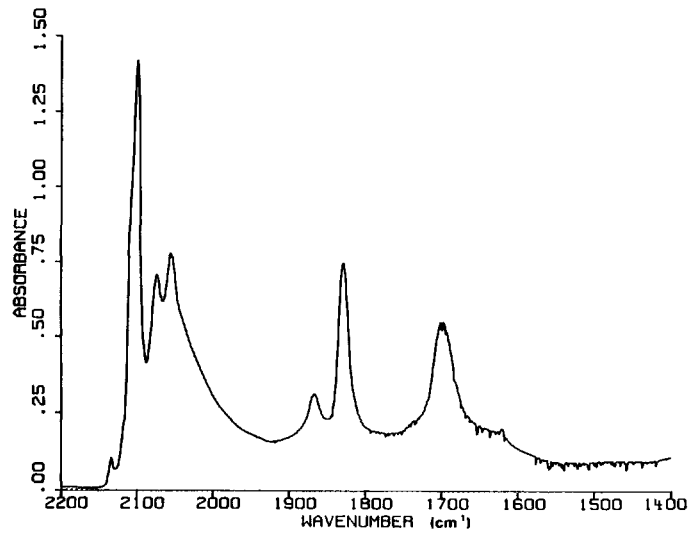

FIG. 6. FTIR spectrum of the carbonyl region of Rh^NMn/NaY.

described in part (a) is the presence of the prominent band at 1699 cm^{-1}, which has been assigned to a mixed carbonyl Rh_n–C–O–Mn^{2+} (38).

(c) Rh^NMn^N/NaY, i.e., a sample that was exposed to NaOH both after the reduction of Rh and after the exchange of Mn, is shown in Fig. 7 after exposure to CO. In this spectrum, only bands ascribed to CO adsorbed on Rh are identifiable, $Rh_6(CO)_{16}$ from the bands at 2097, 2091, 2071, 1871, and 1831 cm^{-1} and possibly $Rh^+(CO)_2$ from contribution at 2025 and 2098 cm^{-1}. No mixed Rh–Mn carbonyl is observed.

5. Extended X-Ray Absorption Fine Structure (EXAFS)

The Fourier transforms of the k^3-weighted EXAFS oscillations $k^3\chi(k)$ of Rh^N/NaY and Rh^NMn^N/NaY calcined

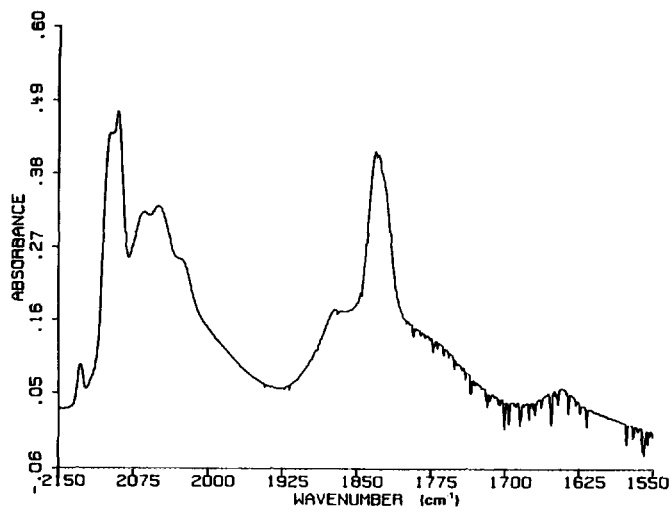

FIG. 5. FTIR spectrum of the carbonyl region of Rh^N/NaY.

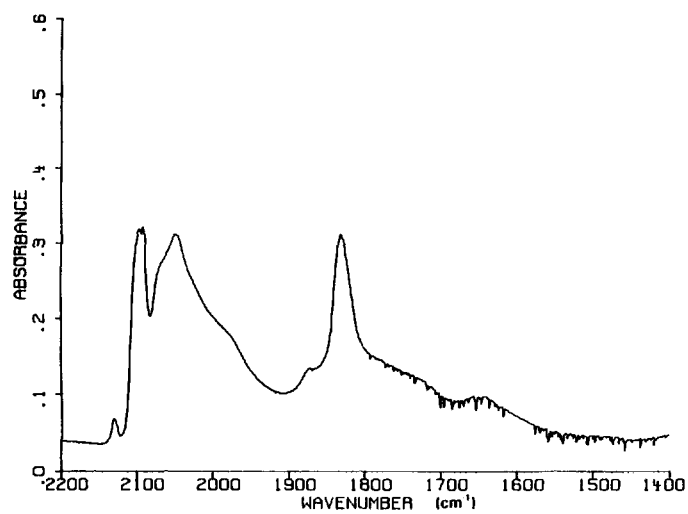

FIG. 7. FTIR spectrum of the carbonyl region of Rh^NMn^N/NaY.

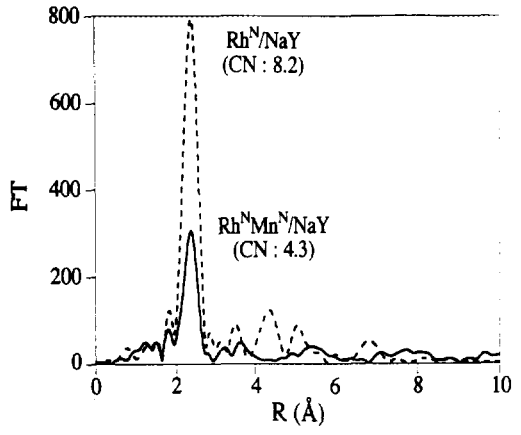

FIG. 8. EXAFS Fourier transform spectra and average coordination number (CN) of Rh^N/NaY and Rh^NMn^N/NaY.

at 400°C and then reduced at 400°C are shown in Fig. 8. A qualitative comparison of both profiles indicates that the coordination number of rhodium is much lower in Rh^N/NaY than in Rh^NMn^N/NaY, as can be seen from the smaller intensity of the Fourier transform peak centered at 0.250 nm (phase not corrected). Correction for the phase shift yields an R_{Rh-Rh} value of 0.265–0.267 nm. The EXAFS parameters of the samples Rh^N/NaY and Rh^NMn^N/NaY are shown in Table 2. The peak intensity is directly related to the average coordination number of Rh and an average particle size can be estimated from the coordination number. It can be seen in the figure that, on average, particles are larger in Rh^N/NaY (about 20 Å in diameter) than in Rh^NMn^N/NaY (about 10 Å).

DISCUSSION

1. Effects of Zeolite Protons on Catalyst Selectivity and the Chemical State of Manganese

The present results show that zeolite protons affect catalyst activity in two important ways. First, they act as active sites catalyzing a secondary conversion of primary oxygenates to other products. This is obvious from a comparison of the product distributions observed in the layered bed experiments; HY downstream of neutralized RhMn/NaY converts primary oxygenates into hydrocarbons, presumably by a mechanism similar to the methanol to gasoline (MTG) process, which is also catalyzed by an acid zeolite. Only after 7 h on stream will some oxygenates break through, possibly because by that time the most active acid sites have become posioned. A chromatographic effect, i.e., adsorption on the second bed of the oxygenates formed in the first one, appears unlikely, as the selectivity towards C_2 hydrocarbons is much higher when the HY bed is placed downstream than in the reversed configuration (23 vs 10%). This suggests that the additional C_2 hydrocarbons observed when the HY bed is placed downstream are secondary products derived from oxygenates reacting at the acid sites. As the time of reaction increases and the acid sites become poisoned, the selectivity towards C_2 hydrocarbons gradually decreases and that toward oxygenates increases.

TABLE 2

Structure Parameters from EXAFS for Samples after *in Situ* Reduction at 400°C[a]

Sample	CN	R (Å)	$\Delta\sigma^2$(Å^2 × 10^{-2})	ΔE_0 (eV)
Rh^N/NaY	4.3	2.65	0.0031	−0.78
Rh^NMn^N/NaY	8.2	2.67	0.0014	−0.14

[a] Notation: CN, coordination number; R, coordination distance; $\Delta\sigma^2$, Debye–Waller factor; ΔE_0, inner potential correction.

A second effect caused by acidic protons concerns the hydrolysis equilibrium of Mn,

$$Mn(OH)_2 + 2\,H^+ \rightleftarrows Mn^{2+} + 2H_2O. \quad [1]$$

By controlling the proton concentration in the zeolite the state of the manganese can be controlled. If proton concentration is high, Mn will be present as Mn^{2+} ions; if it is low, Mn hydroxide is formed, which is converted to MnO_2 during calcination and reduced to MnO in the subsequent reduction treatment. We therefore consider as crucial the results in which catalyst precursors were exposed to an alkaline solution in the critical stage after loading the zeolite with Mn but before exchanging it with Rh. In these samples Rh clusters coexist with MnO particles. When the treatment with alkaline solution is omitted but subsequently the same calcination and reduction conditions are applied, the Mn in the zeolite is present as Mn^{2+} ions. An important condition for this strategy of preparing two further identical catalysts which differ exclusively in the state of the manganese is the prevention of proton formation during reduction of the Rh^{3+} ions. As mentioned, this was achieved by keeping a sufficient number of NH_3 ligands intact during calcination of the $Rh(NH_3)_5(H_2O)^{3+}$-containing catalyst precursor at 200°C.

The results in Fig. 3 thus show the dramatic effect of the chemical state of manganese on the promotion towards the formation of higher oxygenates. When manganese is present as Mn^{2+} ions, no oxygenates are observed, even if zeolite protons have been neutralized by the released NH_3 ligands. However, when Mn^{2+} ions are converted to MnO by treatment with NaOH, followed by calcination and reduction, significant amounts of oxygenates are obtained as products. As the protons are neutralized in both cases, this finding shows that the actual promoter is MnO and *not* Mn^{2+} ions. The TPR data further show that no Mn° is formed under the conditions used; alloy formation between Rh and Mn can thus be disregarded.

2. Nature of the Interaction between MnO and Rh Clusters

The results suggest that the promoting effect of MnO towards formation of higher oxygenates takes place at the rhodium/manganese oxide interface. Independent evidence for direct contact of rhodium with manganese oxide is provided by the TPR, TPD, and EXAFS data.

The TPR profile of Rh^NMn^N/NaY (Fig. 4, trace e) is markedly different from a linear combination of the TPR spectra of Rh^N/NaY (trace c) and Mn^N/NaY (trace b). The same observation has been made in several bimetallic systems, e.g., PtCu/NaY (33), $RhFe/SiO_2$ (39), RhFe/NaY (40), and PdNi/NaY (41). The amount of H_2 consumed is much higher than that required by Rh reduction. This means that manganese oxides are coreduced with Rh. The highest reduction peak in the spectrum is at about 175°C, lower than any of the peaks in the TPR profile of Mn^N/NaY. This remarkable shift to lower reduction temperatures of the manganese oxide strongly suggests that Rh and Mn oxides are in close proximity, e.g., sharing a zeolite cage. Metallic rhodium provides sites for hydrogen adsorption and dissociation of extremely low activation energy. If MnO_x particles are close enough to metal sites, their reduction by atomic hydrogen takes place at a lower temperature than if molecular hydrogen had to interact with MnO_2. This is what appears in Fig. 4. In other words, the reducibility of higher Mn oxides is enhanced by the close proximity of Rh. The lowest-temperature reduction peak, which can be ascribed to the reduction of Rh oxide, is somewhat shifted upward with respect to Mn-free Rh oxide, possibly indicating partial coverage of rhodium oxide with manganese oxide, so that hydrogen has to diffuse through this overlayer.

Hydrogen spillover over large distances has sometimes been invoked as an explanation for enhanced reducibility by the presence of a noble metal (42, 43). We have two reasons for disregarding this phenomenon in the present case: (a) If adsorbed hydrogen atoms on the metal were to migrate over the zeolite surface to the reducible oxide, the energy difference between H adsorbed on Rh and H adsorbed on the bare zeolite wall would create a highly endothermic step. While protons are stable and mobile on zeolites, electrons cannot be easily transported through an insulating oxide. (b) We have studied enhanced reducibility in a number of systems ((Pt + Cu)/NaY (33), (Ni + Pd)/NaY (41), (Re + Pt)/Al_2O_3 (44), (Fe + Pd)/NaY (45), etc.) and always found that close proximity between the reducible species and the reducibility enhancing noble metal was a necessary condition. Once this was given, and reduction to the zerovalent state of the less noble species was thermodynamically allowed, enhanced reduction always resulted in formation of an alloy of both metals. We therefore interpret the present finding that Rh dramatically enhances the reduction of MnO_2 to MnO as evidence for a close proximity between rhodium and the manganese oxide.

Further support for the idea of interacting Rh and MnO clusters is furnished by the EXAFS results. The data in Fig. 8 clearly show that the average coordination number of Rh is significantly lower in Rh^NMn^N/NaY (4.3) than in Rh^N/NaY (8.2). Obviously, the Rh clusters are smaller in Rh^NMn^N/NaY, where they coexist with MnO particles. The presence of MnO thus (a) increases the nucleation rate for Rh during its reduction and/or (b) prevents the migration and secondary growth of primary Rh clusters. In either case the final result is smaller Rh particles. Previous work on RhCr/NaY (46) and PtFe/NaY (47, 48) yielded analogous EXAFS evidence; in all cases the metal particle size is smaller when the metal coexists with a transition element in an oxidized state inside the same zeolite cavities. This phenomenon has been called "chemical anchoring."

At first sight it appears surprising that the H/Rh ratio obtained from H_2 TPD is significantly smaller for Rh^NMn^N/NaY than for Rh^N/NaY (Table 1). As EXAFS unambiguously shows that the smaller H/Rh value in Rh^NMn^N/NaY is *not* caused by a larger size of the Rh clusters, the smaller H/Rh value of Rh^NMn^N/NaY could indicate that the embracing of Rh and MnO is mutual, Rh^0 being anchored but also partially encapsulated by MnO. This suggests a close proximity between Rh and MnO particles. An alternative explanation would be that the propensity of Rh to chemisorb hydrogen decreases with cluster size, as is indeed indicated by measurements of the sticking coefficient of H_2 on small metal clusters in molecular beams (49) and of proton-anchored Rh clusters in zeolite NaHY (50, 51). This is not the place to further speculate on these hypothetical causes; what is relevant for the present study is that the data strongly indicate an intimate interaction between Rh clusters and MnO particles in the catalysts with high selectivity towards oxygenates. It is certain that the Rh–MnO interface is inside the zeolite. Clusters of Rh and MnO particles can either share a supercage or form bridges between adjacent cages. More probably, the Rh/MnO couples are located in voids or mesopores created by growing Rh particles.

The CO-IR spectrum on Rh^NMn/NaY (Fig. 5) shows a band at 1699 cm^{-1} that has been assigned to a mixed carbonyl Rh_n–C–O–Mn^{2+} with "tilted CO" (38), an example of the very close proximity of Rh and Mn^{2+} ions. As expected, this band was not detected in the neutralized catalyst containing all manganese as MnO. It is conceivable that the Rh–CO–Mn^{2+} configuration is easily formed when mobile Mn^{2+} ions can migrate to the appropriate position after CO has been adsorbed on the surface of the Rh_n particles; however, CO molecules cannot penetrate into the interface between particles of MnO and Rh.

3. Mechanism of Higher Oxygenate Formation

The fact that formation of higher oxygenates over Rh catalysts is promoted by MnO but not Mn^{2+} ions suggests that O^{2-} anions play an important role in the promoting effect. This still leaves open two possibilities:

(i) Oxide ions modify the electronic properties of the adjacent Mn^{2+} ions, for instance, changing their Lewis acidity and thereby affecting the catalyst capability to form or stabilize intermediates to higher oxygenates.

(ii) Carbon-oxygen bonds are formed so that the O^{2-} ions from the promoter are incorporated into the oxygenate precursor.

In case (i) the O atom in the oxygenate product, barring secondary exchange, is still attached to the same C atom as in the original CO molecule. For some catalysts Orita *et al.* have shown that the oxygen-carrying carbon atom in acetaldehyde stems from a nondissociative adsorption of CO (15). An acyl group could be the precursor of ethanol or higher alcohols, as has been proposed by several authors (8, 14, 24, 27, 52). In this case the role of the Lewis acid (Mn^{2+}) in the MnO promoter is to activate the C–O bond to the appropriate extent, inviting insertion of alkyl fragments without fully dissociating the CO molecule. Mn^{2+} ions are coordinated to O^{2-} anions both when encaged in the zeolite support and when encaged in an MnO particle, but their immediate environment is clearly different in each case. The observed difference in promoting effect between zeolite-encaged Mn^{2+} ions and MnO particles could then be caused by the different Lewis acidities of the Mn ion in different environments.

In case (ii) a new carbon–oxygen bond is formed with an O^{2-} ion of an MnO particle. Given the evidence that for oxygenate-selective catalysts the main products are ethanol and ethyl acetate, chemical intuition suggests that adsorbed *acetate ions* are likely precursors. Two highly speculative mechanisms for the formation of oxygenates on Rh/MnO pairs are sketched in Figs. 9 and 10. Figure 9 depicts a hypothetical precursor bridging over the Rh–MnO interface. The CO molecule is nondissociatively adsorbed, its C atom interacts with a Rh atom and an oxygen ion of the MnO promoter, while its oxygen atom interacts with the Mn^{2+} ion. This results in a carboxylate-like structure, which is, however, strained, thus inviting

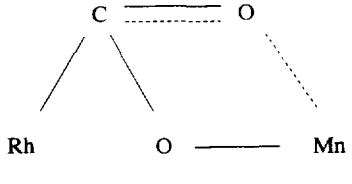

FIG. 9. Hypothetical precursor of higher oxygenates formed by the bridging-mode adsorption of CO on Rh and MnO.

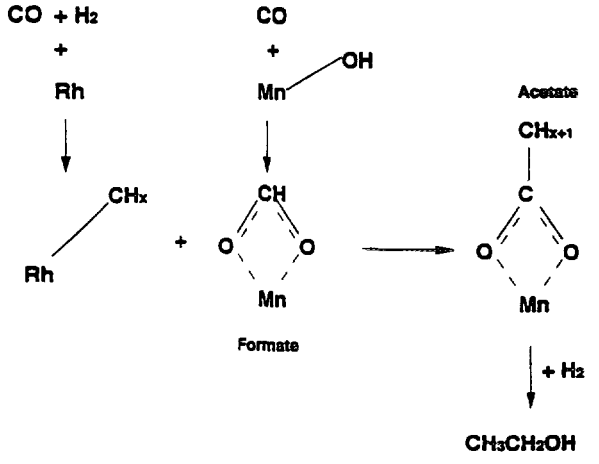

FIG. 10. Hypothetical mechanism of formation of higher oxygenates via interaction of adsorbed species on MnO with those on Rh.

chemical bond formation with an adjacent alkyl group, most likely adsorbed on a Rh ensemble including this Rh atom. After subsequent additions of H atoms, the oxygenate molecule is desorbed.

An alternative mechanism is sketched in Fig. 10. It assumes that adsorbates formed on the rhodium surface interact with other adsorbates on the MnO surface. The rhodium surface is the locus of CO dissociation and of growth of alkyl chains. On the manganese oxide surface adsorption of CO is nondissociative; its insertion into a surface hydroxyl group could result in a surface formate. Interaction between the CH_x on Rh and the surface formate across the Rh–MnO interface might give an acetate. Higher carboxylates will be formed if the alkyl group on the Rh has grown prior to its insertion. Again, H atoms are subsequently added, leading to desorption of the oxygenate molecule.

It is not possible yet to decide between these hypothetical mechanisms. In a recent paper it was also shown that with Fe-promoted Rh catalysts the formation of higher oxygenates occurs only when Fe is present as oxide particles and not as Fe^{2+} ions (40). It thus appears that in catalyst promotion toward formation of oxygenates, the O^{2-} ions surrounding the promotor ion, Mn^{2+} or Fe^{2+}, play a crucial role that has not been identified previously.

ACKNOWLEDGMENTS

We gratefully acknowledge support from the Director of the Chemistry Division, Basic Energy Sciences, U.S. Department of Energy, Grant DE-FG02-87ER13654.

We thank the management of the Cornell High Energy Synchrotron Source for permission to use their facilities for collecting *EXAFS* data and we thank the Wilson Laboratory, Cornell University, for their hospitality and assistance.

REFERENCES

1. Castner, D. G., Blackadar, R. L., and Somorjai, G. A., *J. Catal.* **66,** 257 (1980).
2. Ichikawa, M., *Bull. Chem. Soc. Jpn.* **51,** 2268 (1978).
3. Ichikawa, M., *Bull. Chem. Soc. Jpn.* **51,** 2273 (1978).
4. Van der Lee, G., and Ponec, V., *Catal. Rev. Sci. Eng.* **29,** 183 (1987).
5. Sexton, B. A., and Somorjai, G. A., *J. Catal.* **46,** 167 (1977).
6. Castner, D. G., and Somorjai, G. A., *Surf. Sci.* **83,** 60 (1979).
7. Solymosi, F., and Erdöhelyi, A., *Surf. Sci.* **110,** L630 (1981).
8. Ichikawa, M., *Polyhedron* **7,** 2351 (1988).
9. Underwood, R. P., and Bell, A. T., *Appl. Catal.* **21,** 157 (1986).
10. Kiennemann, A., Breault, R., Hindermann, J.-P., and Laurin, M., *J. Chem. Soc. Faraday Trans. 1* **83,** 2119 (1987).
11. Luo, H. Y., Bastein, A. G. T. M., Mulder, A. A. J. P., and Ponec, V., *Appl. Catal.* **38,** 241 (1988).
12. Ellgen, P. C., Bartley, W. J., Bhasin, M. M., and Wilson, T. P., *Adv. Chem. Ser.* **178,** 147 (1979).
13. Arakawa, H., Hanaoka, T., Takeuchi, K., Matsuzaki, T., and Sugi, Y., *in* "Proceedings, 9th International Congress on Catalysis, Calgary, 1988" (M. J. Phillips and M. Ternan, Eds.) Vol. 2, p. 602. Chem. Institute of Canada, Ottawa, 1988.
14. Sachtler, W. M. H., *in* "Proceedings, 8th International Congress on Catalysis, Berlin, 1984," Vol. 1, p. 151. Dechema, Franfurt-am-Main, 1984.
15. Orita, H., Naito, S., and Tamaru, K., *J. Chem. Soc. Chem. Commun.*, 150 (1984).
16. Chuang, S. C., Goodwin, J. G., Jr., and Wender, I., *J. Catal.* **95,** 435 (1985).
17. Kagami, S., Naito, S., Kikuzono, Y., and Tamaru, K., *J. Chem. Soc. Chem. Commun.*, 256 (1983).
18. Borer, A. L., and Prins, R., *J. Catal.* **144,** 439 (1993).
19. Fukushima, T., Arakawa, H., and Ichikawa, M., *J. Phys. Chem.* **89,** 4440 (1985).
20. Koerts, T., PhD thesis, Eindhoven University of Technology, 1992.
21. Kowalski, J., van der Lee, G., and Ponec, V., *Appl. Catal.* **19,** 423, (1986).
22. Kip, B. J., Smeets, P. A. T., van Grondelle, J., and Prins, R., *Appl. Catal.* **33,** 181 (1987).
23. Van den Berg, F. G. A., PhD thesis, State University of Leiden, 1983.
24. Sachtler, W. M. H., and Ichikawa, M., *J. Phys. Chem.* **90,** 4752 (1986).
25. Chuang, S. S. C., and Pien, S.-I., *J. Catal.* **138,** 536 (1992).
26. Chuang, S. S. C., and Pien, S.-I., *J. Catal.* **135,** 618 (1992).
27. Sachtler, W. M. H., Shriver, D. F., Hollenberg, W. B., and Lang, A. F., *J. Catal.* **92,** 429 (1985).
28. Mori, Y., Mori, T., Hattori, T., and Murakami, Y., *Catal. Lett.* **10,** 171 (1991).
29. Ichikawa, M., and Fukushima, T., *J. Chem. Soc. Chem. Commun.*, 321 (1985).
30. Bastein, A. G. T. M., van der Boogert, W. J., van der Lee, G., Luo, H., Schuller, B., and Ponec, V., *Appl. Catal.* **29,** 243 (1987).
31. Van den Berg, F. G. A., Glezer, J. H. E., and Sachtler, W. M. H., *J. Catal.* **93,** 340 (1985).
32. Treviño, H., and Sachtler, W. M. H., *Catal. Lett.* **27,** 251 (1994).
33. Moretti, G., and Sachtler, W. M. H., *J. Catal.* **115,** 205 (1989).
34. Zhang, Z. C., Xu, L., and Sachtler, W. M. H., *J. Catal.* **131,** 502 (1991).
35. Yin, Y.-G., Zhang, Y. C., and Sachtler, W. H. M., *J. Catal.* **138,** 721 (1992).
36. Schünemann, V., Adelman, B. J., and Sachtler, W. M. H., *Catal. Lett.* **27,** 259 (1994).
37. Rao, L.-F., Fukuoka, A., Kosugi, N., Kuroda, H., and Ichikawa, M., *J. Phys. Chem.* **94,** 5317 (1990).
38. Beutel, T., Knözinger, H., Treviño, H., Zhang, Z. C., Sachtler, W. M. H., Dossi, C., Psaro, R., and Ugo, R., *J. Chem. Soc. Faraday Trans.* **90,** 1335 (1994).
39. Van't Blik, H. F. J., and Niemantsverdriet, J. W., *Appl. Catal.* **10,** 155 (1984).
40. Schünemann, V., Treviño, H., Lei, G.-D., Tomczak, D. C., Sachtler, W. M. H., Fogash, K., and Dumesic, J. A., *J. Catal.* **153,** 144 (1995).
41. Feeley, J. S., and Sachtler, W. M. H., *Zeolites* **10,** 738 (1990).
42. Dmitriev, R. V., Steinberg, K.-H., Detjuk, A. N., Hofmann, F., Bremer, H., and Minachev, Kh. M., *J. Catal.* **65,** 105 (1980).
43. Dmitriev, R. V., Detjuk, A. N., Minachev, Kh. M., and Steinberg, K.-H., *in* "Spillover of Adsorbed Species" (G. M. Pajonk, S. J. Teichner, and J. E. Germain, Eds.), Studies in Surface Science and Catalysis, Vol. 17, p. 17. Elsevier, Amsterdam, 1983.
44. Augustine, S. M., and Sachtler, W. M. H., *J. Catal.* **106,** 417 (1987).
45. Xu, L., Lei, G., Sachtler, W. M. H., Cortright, R., and Dumesic, J. A., *J. Phys. Chem.* **97,** 11517 (1993).
46. Tzou, M. S., Teo, B. K., and Sachtler, W. M. H., *Langmuir* **2,** 773 (1986).
47. Tzou, M. S., Jiang, H. J., and Sachtler, W. M. H., *Appl. Catal.* **20,** 231 (1986).
48. Tzou, M. S., Teo, B. K., and Sachtler, W. M. H., *J. Catal.* **113,** 220 (1988).
49. Andersson, M., Holmgren, L., and Rosén, A., presented at ISSPIC-7, Kobe, Japan, 1994.
50. Tomczak, D. C., Zholobenko, V. L., Treviño, H., Lei, G.-D., and Sachtler, W. M. H., *in* "Zeolites and Related Microporous Materials: State of the Art 1994" (J. Weitkamp, H. G. Karge, H. Pfeifer, and W. Hölderich, Eds.) Studies in Surface Science and Catalysis, Vol. 84, Part B, p. 893. Elsevier, Amsterdam, 1994.
51. Tomczak, D. C. Schünemann, V., Lei, G.-D., and Sachtler, W. M. H., *Microporous Mater.*, in press.
52. Fukushima, T., Arakawa, H., and Ichikawa, M., *J. Chem. Soc. Chem. Commun.*, 729 (1985).